Journal of Membrane Science 733 (2025) 124368

Contents lists available at ScienceDirect

Journal of Membrane Science

journal homepage: www.elsevier.com/locate/memsci

Tuning properties of PEO-functionalized ion-solvating blend membranes via PEO side chain length: Impact on alkaline water electrolysis performance

Sara Gjoshi [a], Charalampos Anastasopoulos [a], Kamal Ghotia [b], Davide Grilli [b], Franz Egert [b,c], Syed Asif Ansar [b], Fatemeh Razmjooei [b,*], Valadoula Deimede [a,**]

[a] Department of Chemistry, University of Patras, GR-26504, Patras, Greece
[b] Institute of Engineering Thermodynamics, German Aerospace Center (DLR), 70569, Stuttgart, Germany
[c] Faculty 6–Aerospace Engineering and Geodesy University of Stuttgart, 70569, Stuttgart, Germany

ARTICLE INFO

Keywords:
Ion-solvating membranes (ISMs)
Alkaline water electrolysis
PEO-Containing polymer
Alkaline stability
Hydrogen cross-over

ABSTRACT

Ion-solvating membranes (ISMs) based on chemical stable polyoxindole copolymers bearing long side PEO groups (MW750) were synthesized via a PEO-functionalization monomer strategy followed by super acid polyhydroxyalkylation. The synthesized copolymer membranes displayed very high electrolyte uptakes even at low KOH concentrations (10 wt%) due to deprotonation of oxindole groups enabling high KOH absorption. However, the increased plasticization resulted in deterioration of mechanical strength and the copolymers were therefore blended with *m*-PBI to yield mechanical robust, nanophase separated ISMs. Their physicochemical properties were tuned by adjusting the blend composition. The prepared blend membranes showed high KOH and water absorption in 30 wt% KOH concentration even higher than that of pure *m*-PBI. The presence of long hydrophilic side PEO chains facilitates both KOH and water uptake due to increased free volume and induced phase separation. This in turn resulted in high ionic conductivity exceeding 100 mS cm^{-1} at 80 °C. Long term stability in 30 wt% KOH at 80 °C for blend PBI80/P(IB-PEO_{750}) was excellent: the conductivity remained unchanged (at room temperature), the thermal stability was improved, while the membrane retained its flexibility and the tensile strength and Young's modulus remained high after the 2 months (1440 h) test. The excellent alkaline stability was attributed to the stabilization of blend membranes via strong attractive electrostatic interactions between *m*-PBI's imidazolide and isatin or PEO groups with K^+. The blend PBI80/P(IB-PEO_{750}) was evaluated under alkaline electrolysis conditions using a 30 wt% KOH feed solution at 80 °C. It exhibited a high current density of 1.06 A cm^{-2} at 1.8 V. In comparison, the corresponding blend with short PEO groups PBI80/P(IB-PEO_{350}) showed higher current density of 1.36 A cm^{-2} at the same voltage, which is comparable to the excellent performance of *m*-PBI. Long-term durability tests revealed that the cell with PBI80/P(IB-PEO_{750}) membrane successfully run for 250 h at 80 °C under a constant current density of 0.5 A cm^{-2}, in contrast to the cell with PBI80/P(IB-PEO_{350}) membrane, which failed after 160 h, showing its applicability in harsh alkaline AWE conditions. In addition, the H_2 in O_2 content for both cells with different blend membranes was low, in the range of 1.4–1.65 vol%, indicating low gas impurities for both cells. This work provides a simple blending strategy for designing chemically stable, with promising performance membranes for alkaline water electrolysis.

1. Introduction

Water electrolysis is the leading technology for high-purity hydrogen production through the electrochemical splitting of water and is essential for the decarbonization of the transportation and industrial sectors when entirely powered by intermittent renewable energy sources (e.g., wind, sea wave, and biomass) [1–3]. The two mature electrolysis technologies operating at low temperatures are traditional alkaline water electrolysis (AWE) and proton exchange membrane water electrolysis (PEMWE) [4–8]. The latter is a promising technology delivering high

* Corresponding author.
** Corresponding author.
E-mail addresses: Fatemeh.Razmjooei@dlr.de (F. Razmjooei), deimede@upatras.gr (V. Deimede).

https://doi.org/10.1016/j.memsci.2025.124368
Received 25 April 2025; Received in revised form 13 June 2025; Accepted 22 June 2025
Available online 23 June 2025

hydrogen production rates at high efficiency but utilizes platinum and iridium as catalysts which are expensive and scarce [8]. In contrast, AWE employs a circulating alkaline solution (30–40 wt.% KOH) and a porous diaphragm membrane thus, enabling the use of low cost, non-platinum metal catalysts (such as Ni foam) and consequently facilitating the cost-effective hydrogen production [2,9]. Despite these significant advantages, AWE has the drawback of typically operating at lower energy efficiency and lower production rate, (with current densities limited to 0.2–0.4 A cm^{-2}), when compared to that of PEMWE that offers more operational flexibility at high current density and efficiency. AWE traditionally operates at low current densities due to high internal ohmic resistance. To enable operation at higher current densities, one effective strategy is to minimize the ohmic resistance, mainly influenced by the ohmic resistance of the diaphragm which can be reduced by replacing a conventional Zirfon separator with an alkaline dense membrane [10].

Recently, anion exchange membranes (AEMs) with improved hydroxide conductivity and stability were proposed for alkaline-based electrolysis conditions [11–13]. For example, Lee and coworkers reported a new category of AEM membranes, a thin film composite (TFC) membrane consisting of an ultrathin quaternary ammonium selective layer formed via Menshutkin reaction-based interfacial polymerization on a porous support [14]. The TFC membrane exhibited high AWE performance (1.16 A cm^{-2} at 1.8 V using Ni based electrodes in 25 wt% KOH) and high durability for 1000 h at 60 °C. It is also reported that ultra-microporous piperidinium containing AEM membranes exhibited high performance, 5.4 A cm^{-2} at 1.8 V and 90 °C, based on precious metal electrodes (Pt/Ru/C as cathode) in low KOH concentration of 1 M, and durability over 2500 h at 60 °C [15]. However, despite the recent substantial conductivity and stability improvements, AEMs are not the best choice for AWE operation conditions, as the high KOH concentration and the elevated temperatures (T > 60 °C) required raise concerns for the stability of AEM membranes. In particular, they suffer from attack on the polymer backbone (if aromatic ether groups are present) and from degradation of fixed cationic groups which are essential for their ion-conducting properties, by nucleophilic substitution and Hofmann elimination [11].

A promising alternative class of membranes for high-rate AWE, are the alkaline ion-solvating membranes (ISMs) as they combine the high conductivity with gas tightness [9]. In contrast to porous diaphragms, ISM are dense (non-porous) polymeric membranes containing polar or ionizable groups in their structure (e.g PVA [16], poly(ethylene oxide) (PEO) [17], imidazoles [18] or benzimidazoles [19–21]), which facilitate the excessive electrolyte absorption and swelling in highly concentrated electrolyte solutions. This in turn leads to the formation of a ternary electrolyte system of polymer/water/KOH, thus enabling OH^- conduction. While the presence of polar or ionazible groups ensures the high ionic conductivity, the lack of fixed cationic groups in their structure promotes alkaline stability. Among different ISMs, poly(2, 2'-(*m*-phenylene)-5,5′-bibenzimidazole) (*m*-PBI) displays high ionic conductivity at 80 °C which increases with increasing KOH concentration (100–200 mS cm^{-1} in 15–25 wt% KOH) [19] and allows for impressive performance characteristics (1.7 A cm^{-2} at 1.8 V at 80 °C) when combined with highly active Ni based electrodes [20]. However, since OH^- conductivity of PBI-based ISMs largely depends on their alkaline absorption capacity, this may be detrimental to the chemical stability of the PBI backbone which is also related to the performance and durability of alkaline electrolyzers. In specific, PBI backbone degradation proceeds via nucleophilic attack at the C2 position of neutral benzimidazole groups which results in ring opening and eventual membrane and cell failure as observed during long term tests at temperatures higher than 60 °C [19,21,22]. With the aim of mitigating backbone degradation, alternative polybenzimidazole chemistries with steric groups situated in the vicinity of vulnerable linkages have been investigated as separators in alkaline water electrolysis [23,24]. New binaphthalene based *m*-PBI (NPBI) showed improved alkaline stability due to the introduction of bulky, rigid binaphthyl moieties next to benzimidazole groups and AWE performance reached a current density of 0.75 A cm^{-2} at 2.0 V in 6 M KOH at 80 °C [24]. In addition, other polymer families derived from aromatic backbones devoid of ether linkages or other polarized bonds in order to avoid backbone degradation including poly(arylene alkylene)s [18], styrene-ethylene-butylene copolymers [25], polyphenylenes [26] and polyisatin [27] and its blends with *m*-PBI [17,28] have been recently reported. Particularly, Hu et al. [27] synthesized a novel and highly stable polymer based on poly (oxindole biphenylene) which showed durable alkaline electrolysis over 2500 h at 80 °C and high operating voltages of 2.3 V. The exceptionally high alkaline stability is associated with the higher energy of the lowest unoccupied molecular orbital (LUMO) of deprotonated oxindole units [27,29] compared to the highest occupied molecular orbital (HOMO) energy of OH^-. As recently reported by our group, blending of a chemical robust PEO tether polyoxindole derivative with *m*-PBI had a positive effect on the long-term stability in 20 wt% KOH solution and under real electrolysis cell test conditions [17]. In particular, aryl-ether free aromatic backbone copolymers containing oxindole (isatin) segments and ion-solvating, short PEO chains with molecular weight (MW) of 350 were blended with *m*-PBI and showed high ionic conductivities (110 mScm^{-1} at 80 °C) and excellent alkaline stability for 1 month in 20 wt% KOH at 80 °C as evidenced by preserving their initial mechanical strength and 96–98 % of their original conductivity [17]. The excellent alkaline stability was attributed to the strong attractive interactions developed between *m*-PBI's imidazolide groups and isatin and/or PEO groups of copolymers.

In this work we report the synthesis of new copolymers bearing oxindole and PEO groups with increased side length (MW 750) via super acid-catalyzed polyhydroxyalkylation of biphenyl, isatin and chemically stable PEO side functionalized *p*-terphenyl. Tethering longer side PEO groups on hydrophobic polyoxindole based backbone is expected to promote electrolyte uptake by hindering the close packing of polymeric chains and thereby leading to increased free volume which in turn modulates the ionic conductivity. In addition, the increased PEO content could facilitate both water and electrolyte uptake since ether groups can solvate K^+ ions via acid-donor interactions and can also interact with water via hydrogen bonding. Indeed, the prepared copolymer P(IB-PEO_{750})-*20* displayed very high electrolyte absorption which resulted in extensive swelling and structural softening. To mitigate stability issue, it was blended with *m*-PBI to afford macromolecular reinforced ISMs. The physical properties, alkali absorption, conductivity, mechanical properties, morphology and ex-situ alkaline stability of the prepared blend membranes were systematically investigated, compared to *m*-PBI and PBI80/P(IB-PEO_{350}) membranes fabricated under the same conditions. To elucidate the structure-properties performance relationship, both PBI80/P(IB-PEO_{750}) and PBI80/P(IB-PEO_{350}) blend membranes (having the same composition but different PEO side chain length, MW750 and MW350, respectively) were tested under electrolysis conditions in 30 wt % KOH and characterized with respect to polarization performance, gas purity and durability.

2. Experimental

2.1. Materials

m-PBI powder was supplied by Blue Word Technologies. Poly (ethylene oxide) methyl ether tosylate, 2,5-dibromohydroquinone and 2,5-dibromo-1,4-bis(methoxy poly(ethylene oxide)) benzene were synthesized according to our previously published work [30,31]. Poly (ethylene glycol) methyl ether MW 350 and 750 (98 %, Sigma-Aldrich), benzeneboronic acid (98 %, Alfa Aesar), potassium carbonate (K_2CO_3, 99 %), sodium carbonate (Na_2CO_3, 99 %, Chem-Lab NV), p-toluenesulfonyl chloride (TsCl, 98 %, Sigma-Aldrich), isatin (98 %, Alfa Aesar), biphenyl (99 %, Alfa Aesar), trifluoracetic acid (TFA, 99 %, Alfa Aesar), trifluoromethanesulfonic acid (TFSA, 99 %, Fluorochem), potassium

hydroxide (+85 % pellets, Merck), N,N-dimethylacetamide (DMA, 99.5 %, Scharlab), toluene (Scharlab), *Tetrahydrofuran* (*THF,* Sigma Aldrich), ethyl acetate (Sigma Aldrich), methanol (Sigma Aldrich), dichloromethane (Scharlab), chloroform-*d* (99.80 atom% Deutero DE), dimethyl sulfoxide-d_6 (99.80 atom% Deutero DE), were all used as received without further purification.

2.2. Synthesis of PEO_{750} side functionalized p-terphenyl monomer

The synthesis process was according to the previous reported work [17] and the detailed synthesis steps of the PEO_{750} side functionalized p-terphenyl monomer were described in the Supporting Information (SI).

2.3. Synthesis of P(IB-PEO_{750})-x copolymers

The synthesis of aromatic copolymers bearing isatin and PEO (MW750) side functionalities was performed via super-acid catalyzed polymerization following the previous reported work, with minor modifications [17]. Typically, for the synthesis of P(IB-PEO_{750})-*20* copolymer, isatin (0.809 g, 5.5 mmol), biphenyl (0.617 g, 4 mmol), PEO_{750} side functionalized p-terphenyl monomer (0.615 g, 1 mmol) and TFA (6.11 mL) were added to a dry degassed flask, cooled to 0–5 °C using an ice bath and stirred for 0.5 h. Afterwards, TFSA (7.1 mL) was added into the mixture dropwise. The mixture was stirred vigorously at 0 °C for 2 h and then at room temperature for approximately 4 h to obtain a highly viscous dark-green solution. Subsequently, it was precipitated into methanol to afford a light brown powder polymer. The polymer was thoroughly washed with DI water and finally dried overnight in vacuum oven at 60 °C and isolated in 98 % yield. The synthesized copolymers are denoted as P(IB-PEO_{750})-*x*, where *x* indicates the molar percentage of PEO_{750} side functionalized *p*-terphenyl monomer while IB abbreviation refers to Isatin-Biphenyl segment.

The synthesis of the corresponding aromatic copolymer containing isatin and short PEO chains with MW350 (P(IB-PEO_{350})-*20*) was also carried out and was similar to that of P(IB-PEO_{750})-*20*. The detailed synthetic procedure has been documented previously in the literature [17].

2.4. Blend membrane preparation

The solution-casting method was selected for blend membrane fabrication. To achieve a homogeneous blend solution, P(IB-PEO_{750})-*20* and *m*-PBI were dissolved separately in DMAc (5 wt%) and then mixed at the desired ratios of 70 and 80 wt% *m*-PBI content. The combined solution was filtered through filter paper and cast onto a clean glass substrate of 20 × 20 cm in an oven at 80 °C for 24 h. Subsequently, the polymer film was peeled off from the glass surface, submerged in DI water for 12 h, and then dried in a vacuum oven at 90 °C for 48 h. The thickness of the prepared blend membranes is 100 ± 5 μm. The blend membrane with 80 wt% *m*-PBI and 70 wt% *m*-PBI were denoted as PBI80/P(IB-PEO_{750}) and PBI70/P(IB-PEO_{750}), respectively.

The blend membrane PBI80/P(IB-PEO_{350}) (80 wt% of *m*-PBI and 20 wt% of P(IB-PEO_{350})-*20*) was prepared following the as described procedure.

2.5. Characterization

The proton Nuclear Magnetic Resonance (^{1}H NMR) spectra were recorded at 25 °C on an Advance DPX 600 MHz spectrometer (Bruker) in DMSO-d_6 or $CDCl_3$. The chemical shifts are reported relative to tetramethylsilane (TMS) which was used as internal standard. Attenuated Total Reflection Fourier Transform Infra-Red (ATR-FTIR) spectra were collected on a Platinum ATR spectrometer (Bruker) in the spectral range from 4000 to 400 cm^{-1} with a resolution of 4 cm^{-1}. Thermogravimetric analysis (TGA, Labsys TG, Setaram Instrumentation) was carried out in the temperature range from 25 to 800 °C under nitrogen atmosphere at a heating rate of 20 °C min^{-1}. X-ray diffraction (XRD) was performed using a Bruker D8 Advance diffractometer equipped with a Cu source (λ = 1.54 Å) in the range of 5–60° 2θ at a scan speed of 0.5° min^{-1} and a step size of 0.019°. The cross-surface imaging was conducted via Field Emission Scanning Electron Microscopy (FE−SEM, FEI InspectTM F50), using the SE detector. The samples were prepared by fracturing the membranes in liquid nitrogen. GPC measurements were conducted on a Polymer Lab chromatographer equipped with a UV detector and two PLgel 5 μm mixed columns at 25 °C using $CHCl_3$ as eluent with a flow rate of 1 mL min^{-1}. Mechanical properties including tensile strength, elongation at break and Young's modulus were recorded by a Precision Universal/Tensile Tester (Autograph AGS-X, Shimadzu) at a cross speed of 10 mm min^{-1} at room temperature. For each membrane, a minimum of six identical samples were analyzed, and the average value was selected.

Contact angle measurements were recorded using the sessile drop method on a static contact angle computing device (OCA 15 Plus, Data Physics Instruments). After deposition of deionized water droplets of ~12 μL on the dry membrane samples, digital photographs of the water droplets were taken. The average of three measurements for each sample was reported.

2.6. Membrane composition and swelling behavior

The electrolyte uptake and the KOH/water weight fractions of the ion solvating membranes were determined gravimetrically using the method described previously [32]. Membrane samples were immersed in 20, 25 or 30 wt% aqueous KOH solution for 18 h at 80 °C. After careful blotting with a tissue paper, their doped weight was recorded (m_{wet}). Next, the samples were dried in the vacuum at 110 °C for 4 h and their weight (w_{dry}) was recorded. Then KOH was removed by immersion in demineralized water until the pH remained neutral, and the membranes were again dried in the vacuum at 110 °C, and their corresponding weight was recorded ($w_{dedoped}$). The weight fractions of polymer blend (WF_p), KOH (WF_{KOH}) and water (WF_w) were calculated according to the following equations (1)–(3):

$$WF_p(\%) = \frac{m_{dedoped}}{m_{wet}} \times 100 \quad (1)$$

$$WF_w(\%) = \frac{m_{wet} - m_{dry}}{m_{wet}} \times 100 \quad (2)$$

$$WF_{KOH}(\%) = \frac{m_{dry} - m_{dedoped}}{m_{wet}} \times 100 \quad (3)$$

The electrolyte uptake and the concentration of the absorbed KOH solution were calculated by Equations (4) and (5):

$$\text{Total uptake } (\%) = \frac{WF_w + WF_{KOH}}{WF_p} \times 100 \quad (4)$$

$$\text{Concentration of absorbed solution } (\%) = \frac{WF_{KOH}}{WF_w + WF_{KOH}} \times 100 \quad (5)$$

The swelling ratios SR_a and SR_t were determined based on the measured area (*a*) and thickness (*t*) before (dry dimensions) and after doping (wet dimensions) in 20, 25 or 30 wt% aqueous KOH solution for 18 h at 80 °C. The swelling ratios were then calculated according to Equations (6) and (7):

$$SW_a(\%) = \frac{a_{wet} - a_{dry}}{a_{dry}} \times 100 \quad (6)$$

$$SW_t(\%) = \frac{t_{wet} - t_{dry}}{t_{dry}} \times 100 \quad (7)$$

where a_{wet} and a_{dry} are the surface areas of the wet and dry membranes,

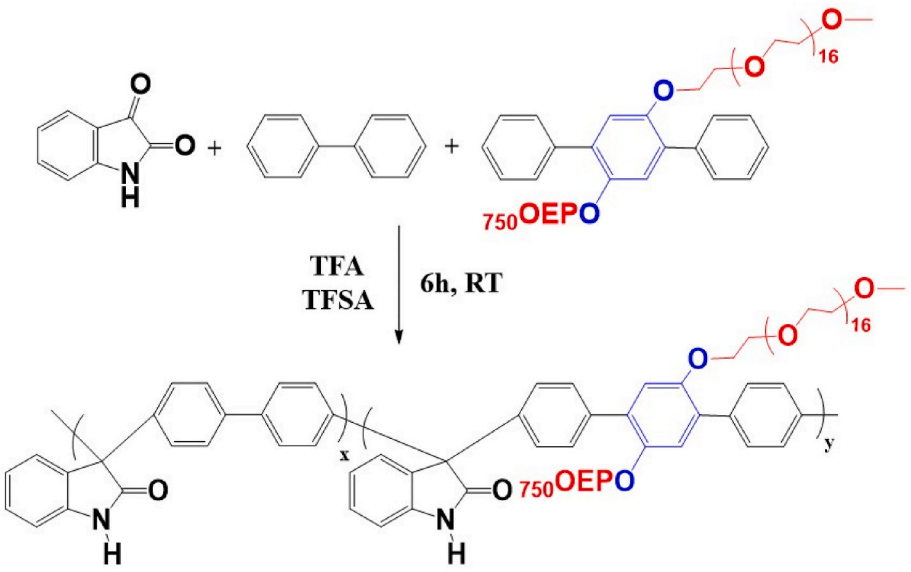

Scheme 1. Synthesis of P(IB-PEO_{750})-*x* copolymers.

and t_{wet}, t_{dry} are the thicknesses of the wet and dry membranes, respectively.

2.7. Ionic conductivity

The through plane ionic conductivity of the membranes was determined by AC impedance spectroscopy at 20, 40, 60, 80 °C. The conductivity measurements were performed using a home-made Teflon cell on AUTOLAB electrochemical workstation (PGSTAT 302 N) equipped with a frequency response analyzer, operating over a frequency range of 10 Hz–1000 kHz. The membranes were placed between two perforated plate nickel electrodes of active area 4 cm^2 and sealed using two Teflon gaskets adjusted to match the membrane thickness in order to prevent mechanical damage caused by compression. The cell was filled with 20 wt% or 30 wt% KOH. Prior to conductivity measurements, the samples were equilibrated in the respective doping solution at 80 °C for 18 h. The ionic conductivity was calculated according to Equation (8), where *l* is the thickness of the doped membrane, *A* is the active area of the electrodes and *R* is the ohmic resistance between the electrodes (taken as the intercept with the real axis of the Nyquist plot).

$$\sigma = \frac{l}{\mathrm{A\ x}\ R} \tag{8}$$

For each membrane, two samples were measured and the average value of the two measurements was reported.

2.8. Alkaline stability

The alkali stability was evaluated after immersion of the blend membranes in 30 wt% aqueous KOH solutions at 80 °C for 1440 h. This experiment was done in sealed PTFE vials to avoid CO_2 adsorption and glass dissolution. The changes in ionic conductivity, mechanical properties, thermal stability were recorded while molecular structure changes were studied using ATR-FTIR spectroscopy.

2.9. Electrolysis testing

For the full cell testing, Ni-based thermal sprayed electrodes of 4 cm^2 active area were used [10]. The zero-gap electrolyzer cell consists of four main parts: Ni bipolar plates, Ni wire mesh as gas/liquid diffusion layers, membranes and Raney Ni-based electrodes. Prior to cell assembly, membranes were soaked in a bath of 30 wt% KOH for 24 h. KOH-doped membranes were placed between two electrodes and supported from each side by gas diffusion layers and fixed by Ni bipolar plates from both sides. The tests have been carried out in atmospheric pressure in 30 wt% KOH at 80 °C, using a BioLogic potentiostat. After 30 min of activation at a constant current of 0.2 A, polarization curves up to 2 A cm^{-2} with a scan rate of 10 mA s^{-1} were recorded. Electrochemical impedance spectroscopy (EIS) was performed at high current density of 2 A cm^{-2} and scanned from 50 kHz to 100 mHz to identify the ohmic and activation losses. The operating conditions and cell hardware were kept the same for all the tests. The equivalent circuit for fitting consisted of lumped resistance (R_{ohm}) in series with two circuits, each comprising a resistance (R cathode (R_c) and R anode (R_a)) and a constant phase element (CPE1 for cathode and CPE2 for anode) in parallel to each other. The inductor (L) in series with the R_{ohm} represents possible inductive parts of cables and other components. The Nyquist plot fitting was performed using RelaxIS software, considering the partially high-frequency tail extending toward positive imaginary parts. This feature is attributed to an inductive contribution from electronics and wiring. The resistance values reported were obtained from the fitting. With this partially inductive effect included, a slight shift in the resistance values obtained from fitting could be observed. At very low frequencies significant residuals were observed. The residuals were scattered randomly in positive and negative directions, which suggested that they were caused by noise. As this noise becomes dominant, fitting was no longer possible in this frequency range, therefore, the noisy section was excluded from fitting. Therefore, EIS fitting was performed in optimal range from 10 kHz to 30 Hz. The long-term durability tests for cells with both different membranes PBI80/P(IB-PEO_{350}) and PBI80/P(IB-PEO_{750}) were done in 30 wt% KOH at 80 °C initially starting with harsh accelerated stress test (AST) followed by operating at constant current density of 0.5 A cm^{-2}. AST was done for duration of 24 h, in which the cell was cycling between low and high current densities of 0.05 and 1.8 A cm^{-2} with the scan rate of 116 mA s^{-1}. Each current density was kept constant for 4 min. The hydrogen crossover was determined in a separate experiment. For this, a 25 cm^2 cell was assembled and placed in the test system. The separators on each side were filled with 1L of 30 wt% KOH. The electrolyte streams of the anode and cathode are mixed to avoid a concentration build up. The electrolyte temperature is set to 80 °C. To determine the impurity, the gas from the separators is cooled down in a gas cooler, where the condensate is removed and fed back into the system. The dried gas on each side flows through a gas quality sensor, specifically tuned for each side's gas

Table 1
Molecular characteristics and physical properties of polyoxindole based copolymers.

Copolymer	M_wPEO	PEO content (wt.%)	Copolymer Composition x/y (mol%)	^{1}H NMR composition x/y (mol%)	EU (%)[a]		M_n	M_w
					20 wt%	30 wt%		
P(IB-PEO$_{750}$)-*20*	750	51.3	80/20	79/21	78	65	92000	164000
P(IB-PEO$_{750}$)-*30*	750	59.6	70/30	71/29	40	26	–	–
P(IB-PEO$_{350}$)-*20*	350	32	80/20	80/20	45 [17]	30	47300	160800

[a] Measured after doping at 80 °C.

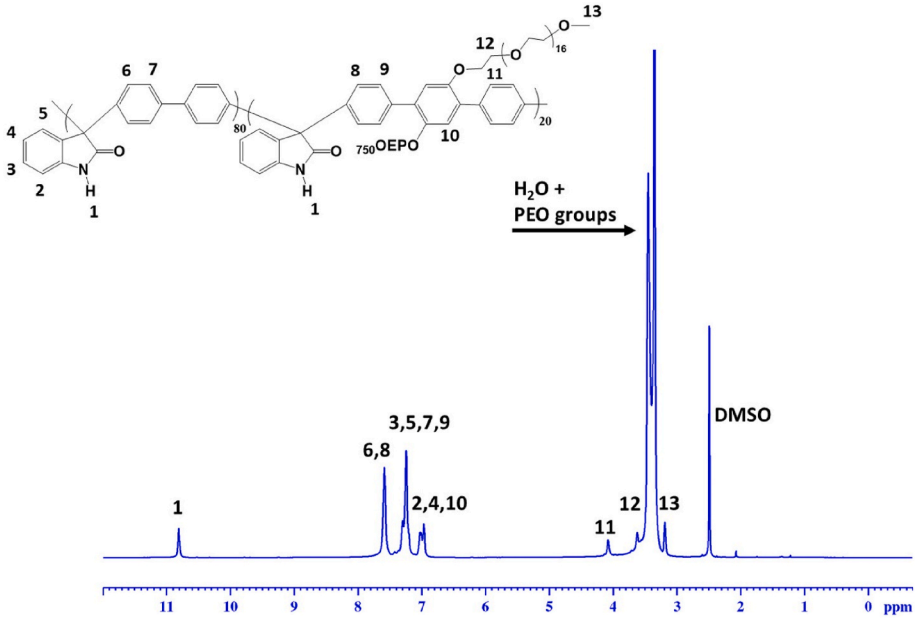

Fig. 1. ^{1}H NMR spectrum of P(IB-PEO$_{750}$)-*20* copolymer in DMSO-d_6.

mixture. The impurity is measured at current densities from 0.7 to 0.05 A cm^{-2} with several current steps. The test started with the highest current density and while the current density of the steps decreases, the duration of the steps increased to compensate for the longer time until equilibrium is reached, due to the lower gas production rate.

3. Results and discussion

3.1. Monomer, polymer synthesis and characterization

The development of durable and high-performing ion-solvating membranes operating in highly concentrated KOH solutions (e.g. 30 wt % KOH) in order to take advantage of the improved electrode performance [33], and the decreased H_2 crossover due to the lower H_2 solubility at higher KOH concentration [34] is a big challenge. At that end, new aryl-ether free backbone copolymers bearing oxindole and longer PEO side moieties (with increased PEO contents) were prepared. In particular, the PEO side-functionalized p-terphenyl with longer PEO side length (MW 750) monomer was copolymerized with isatin and biphenyl via super-acid catalyzed polycondensation to afford copolymers containing high PEO contents.

The synthesis of the PEO$_{750}$ side functionalized p-terphenyl monomer was carried out according to our previous work [17] and followed a three-step synthetic route, as depicted in Scheme S1 of SI. The chemical structure and purity of the synthesized monomer was verified by ^{1}H NMR. As shown in Fig. S1, the signals of aromatic protons were observed between 7.00 and 7.60 ppm. The strong signal in the region of 3.52–3.63 ppm is attributed to the –CH_2– protons of the repeating PEO units, while the peaks at 4.05 ppm and 3.73 ppm correspond to the –CH_2– protons in α and β position to the phenolic oxygen, respectively. Moreover, the signal at 3.36 ppm is assigned to the terminal –OCH_3 groups of the PEO chain [31,35].

Polyoxindole based aryl-ether free backbone copolymers P(IB-PEO$_{750}$)-*x* (Scheme 1) were successfully synthesized by super-acid catalyzed polyhydroxyalkylation of isatin, biphenyl and PEO$_{750}$ side functionalized p-terphenyl, according to the method described elsewhere [36,37]. Two copolymers with 20 and 30 % molar percentages of PEO side functionalized *p*-terphenyl (corresponding to 51.3 and 59.6 wt % PEO, respectively) were synthesized (Table 1). For comparison, the copolymer (P(IB-PEO$_{350}$)-*20* containing shorter PEO groups (MW350) with 20 % molar percentages of PEO side functionalized *p*-terphenyl (corresponding to 32 wt% PEO content) was also synthesized according to previous work [17] and its properties are shown in Table 1.

The chemical structure of the prepared copolymers was confirmed by ^{1}H NMR spectroscopy. Fig. 1 shows the ^{1}HNMR spectrum of P(IB-PEO$_{750}$)-*20* copolymer (DMSO-d_6 was used as a solvent). The N–H proton of isatin appeared at 10.80 ppm (**1**), while the protons in the aromatic region originated from biphenylene and terphenylene segment [17,38]. The central peak at 3.45 ppm is attributed to the methylene protons of the PEO chain. The peaks at 4.10 and 3.65 ppm are ascribed to the –CH_2- protons (**11**, **12**), and the peak at 3.20 ppm is assigned to the terminal –CH_3 groups adjacent to oxygen of the PEO side chains (**13**). In addition, the actual composition of the synthesized copolymers and thus the PEO molar ratio was calculated by comparing the integral area of the isatin proton (**1**) with that of PEO protons (**11**). The PEO molar percentage estimated from the ^{1}H NMR (Table 1) closely correlates with the feed composition of the monomers used in the polymerization reaction. ATR spectroscopy was also studied to confirm the chemical structure of the prepared copolymers. Fig. S2 of SI illustrates the ATR spectra of both P(IB-PEO$_{750}$)-*20* and P(IB-PEO$_{750}$)-*30*

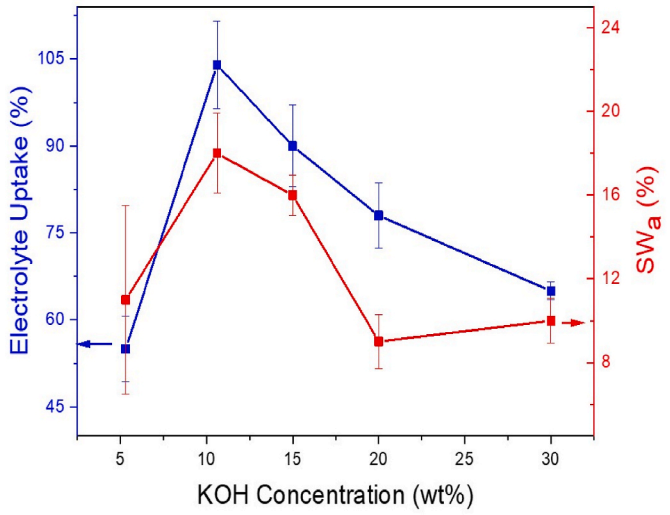

Fig. 2. Total uptake (EU%) and area swelling behavior of P(IB-PEO$_{750}$)-*20* copolymer after equilibration in KOH solutions of different concentrations.

copolymers. The broad absorption band located at 3472 cm^{-1} is assigned to the N–H stretching of isatin, while the characteristic band at 1715 cm^{-1} is attributed to the C═O stretching of the amide bond [17,38,39]. The peaks at 2872 cm^{-1} and 1615 cm^{-1}, are ascribed to the stretching vibration of methylene groups of PEO chain and the C═C stretching vibration of benzene ring [17], respectively.

Both P(IB-PEO$_{750}$)-*20* and P(IB-PEO$_{750}$)-*30* were readily soluble in a wide range of organic solvents such as N-methylpyrrolidone (NMP), *N*, *N*-dimethylformamide (DMF), *N*,*N*-dimethylacetamide (DMAc) and dimethylsulfoxide (DMSO) but only P(IB-PEO$_{750}$)-*20* had good solubility in chloroform, enabling its molecular weight measurement by gel permeation chromatography (GPC). Specifically, P(IB-PEO$_{750}$)-*20* exhibited high molecular weights (M_n = 92,000, Table 1) facilitating the formation of transparent, mechanically robust membranes upon casting from a 5 wt% DMAc solution on a glass substrate. Both copolymers displayed excellent film-forming ability, as evidenced in Fig. S3a and S3b of SI, although P(IB-PEO$_{750}$)-*30* due to its higher PEO content (59.6 wt%) is softer. This is due to the plasticization of the rigid polymer matrix induced by the incorporation of flexible side PEO units. Consequently, the increasing PEO content results in copolymers with increasing structural softness [30].

Thermogravimetric analysis results (Fig. S4 of SI) showed a typical two-stage degradation process for P(IB-PEO$_{750}$)-*20* copolymer which was used as a representative example. An initial weight loss (~2 wt%) up to 165 °C was observed, which was attributed to the absorbed traces of water and/or residual DMAc solvent. The first degradation step began at around 300 °C, ascribed to the loss of PEO side groups, which agrees well with other PEO containing polymers [17,30]. The second weight-loss step was observed at about 470 °C corresponding to the polymer backbone decomposition which is in line with *other ether-free* backbone based *AEM* chemistries reported in literature [17,38]. The data indicates that the prepared copolymers have high thermal stability, adequate for the needs of alkaline water electrolysis.

One of the key characteristics of these ion-solvating copolymer membranes is their capacity to deprotonate in KOH solution to form oxindole anions and subsequently the corresponding ion pairs with potassium, which facilitate the absorption and the transport of hydroxide ions. The absorption of electrolyte could be further supported by hydrophilic PEO groups which can interact with water and can solvate K^+ via acid-base interactions. The electrolyte uptake (EU) of the

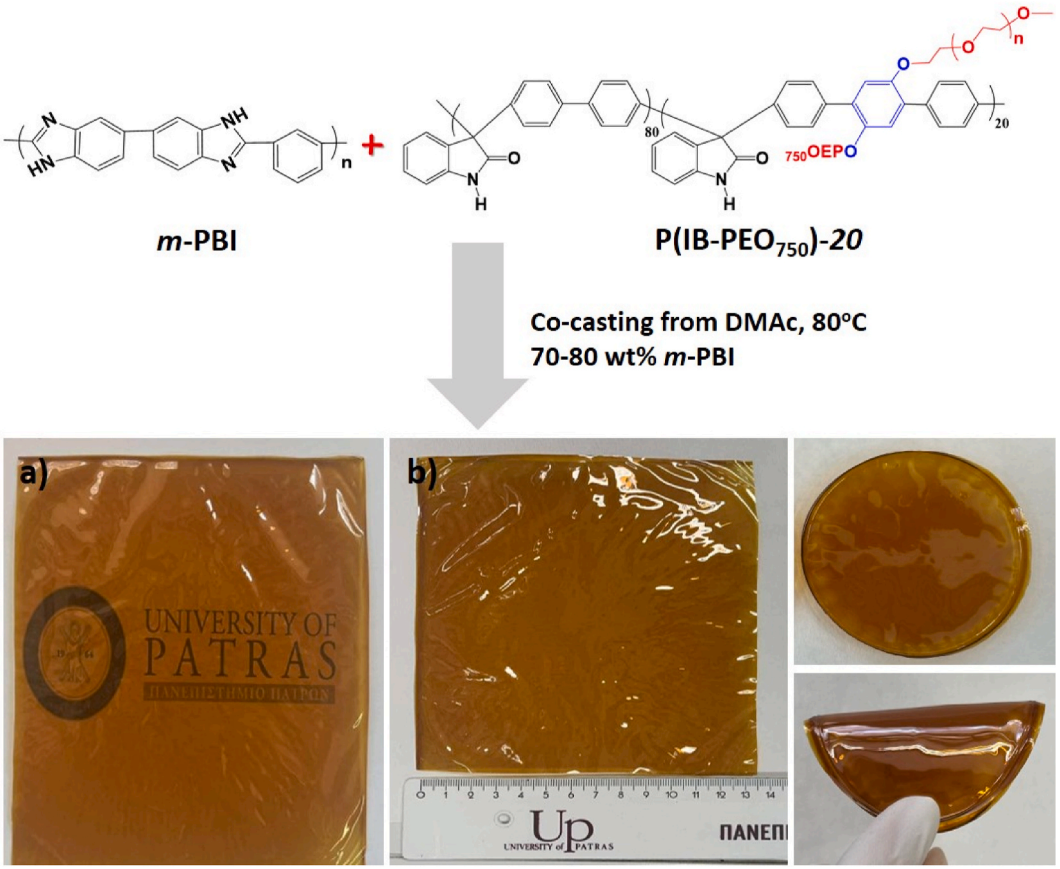

Fig. 3. Chemical structure of *m*-PBI and P(IB-PEO$_{750}$)-*20* and photographs of the flexible prepared blend membranes with different compositions a) 80/20, b) 70/30.

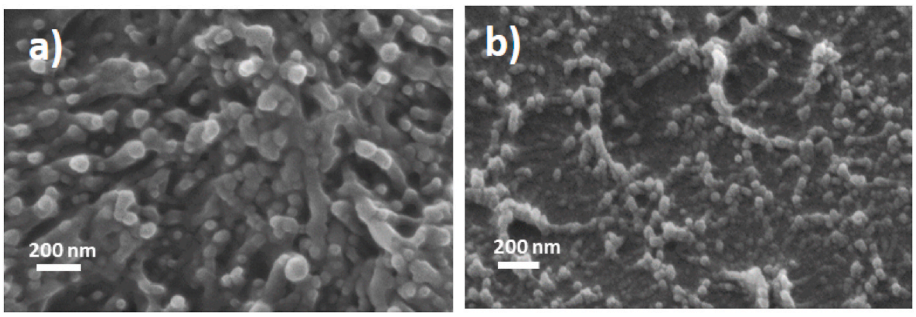

Fig. 4. Cross-sectional SEM micrographs of blend membranes a) PBI80/P(IB-PEO_{750}) and b) PBI70/P(IB-PEO_{750}).

prepared P(IB-PEO_{750})-*20* was studied after doping in 5–30 wt% KOH solutions as shown in Fig. 2 and Table 1.

The electrolyte uptake peaked at 104 % in 10 wt% KOH concentration and thereafter declined with increasing KOH concentration, suggesting that it is readily deprotonated even at very low KOH concentration to form negatively charged potassium oxindole groups along the backbone (pka = 10,83 in water) [28]. This in turn enhances the polarity of the copolymer which could facilitate electrolyte uptake, however, may be compensated by the electrostatic repulsion of OH^- ions owing to Donnan exclusion. The electrolyte uptake decrease with increasing KOH concentration was also observed in AEMs and was attributed to the breakdown of the Donnan exclusion at high enough KOH concentration, resulting in absorption of concentrated electrolyte and shrinking of hydrophilic domains [40]. The area swelling behavior of the copolymer followed the same trend with electrolyte uptake, where the highest swelling ratio (18 %) was observed at KOH concentration of 10 wt %. Both KOH and water weight fractions peaked at 16 wt% and 41 wt% in 10–20 wt% KOH, respectively. These values were higher than those of similar poly(oxindole biphenylenes), which showed a peak at 13.45 wt% and 23 wt% in 6 M KOH (ca. 27 wt%), respectively [27]. These results suggest that not only oxindole groups, but hydrophilic PEO groups also have ion-solvating properties thus leading to increased KOH and water weight fractions.

At the high KOH concentration of 20–30 wt%, which is of interest for alkaline electrolysis systems, copolymer P(IB-PEO_{750})-*30* with the highest PEO weight content (59.6 %), although showed lower electrolyte uptakes (Table 1) compared to P(IB-PEO_{750})-*20* copolymer, was severely plasticized and shrunk due to its softer nature before KOH doping. In summary, the high electrolyte uptakes of both copolymers resulted in extensive plasticization and softening, particularly for P(IB-PEO_{750})-*30* (Fig. S3c and S3d), which in turn led to poor dimensional stability.

3.2. Blend membrane preparation and characterization

Tethering longer side PEO groups with increased PEO content on a hydrophobic aryl-ether free backbone was a successful route to improve EU since the synthesized copolymers showed very high EU at the expense of mechanical strength due to their severe plasticization. To counteract softening of the membranes and increase dimensional stability, P(IB-PEO_{750})-*20* was blended with a mechanically stable matrix *m*-PBI. Two blend membranes containing 20 and 30 wt% of P(IB-PEO_{750})-*20* copolymer were prepared after casting in DMAc solution. Visually homogeneous, transparent and flexible large area membranes were fabricated (20 × 20 cm^2), as illustrated in Fig. 3, highlighting their excellent mechanical properties.

The ^{1}H NMR spectrum of the blend membrane PBI80/P(IB-PEO_{750}), as depicted in Fig. S5 of SI, confirms the presence of both polymers. To verify the possible compatibility of blend membranes, the two membranes were further investigated by SEM (Fig. 4). The cross sections of cryo-fractured membranes are shown in Fig. 4a and b, where a distinct nanophase separation was observed. In both blends, spherical hydrophilic structures consisting mainly of PEO groups (with an average size of 25–60 nm) [7] were dispersed in a hydrophobic matrix comprised *m*-PBI and copolymer backbone. The formation of continuous, hydrophilic structures especially in the hydrated form enables the interconnection of ion transport channels, thus facilitating ion conduction within the blend membranes.

3.2.1. Physicochemical characterization

The electrolyte uptake increased continuously with increasing KOH concentration (20–30 wt%) for PBI80/P(IB-PEO_{750}) and peaked at 150 % in 30 wt% (Fig. 5a) following the typical behavior of KOH-doped *m*-PBI. On the other hand, PBI70/P(IB-PEO_{750}) showed a maximum electrolyte uptake value of 144 % in 25 wt% while with further increase of KOH concentration to 30 wt%, the electrolyte uptake declined to 127 % (Fig. 5a) mostly due to the decreasing water activity with KOH

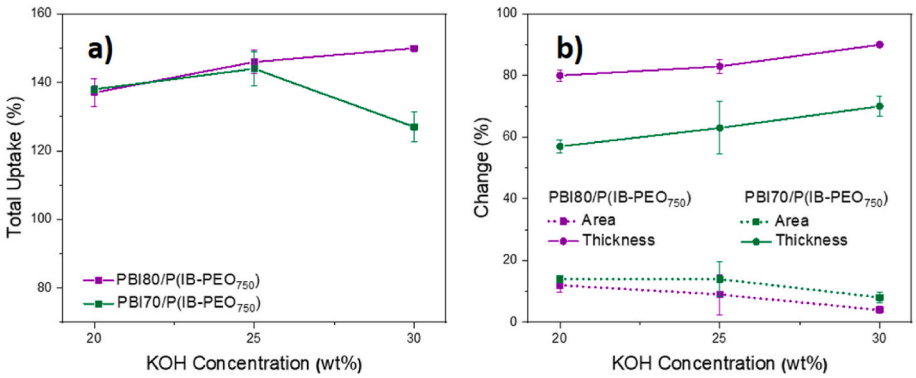

Fig. 5. a) Electrolyte uptake and b) dimensional changes of the blend membranes as recorded in aqueous KOH with concentrations of 20–30 wt% at 80 °C. The markers show the average of three samples, and the error bars represent the standard deviation.

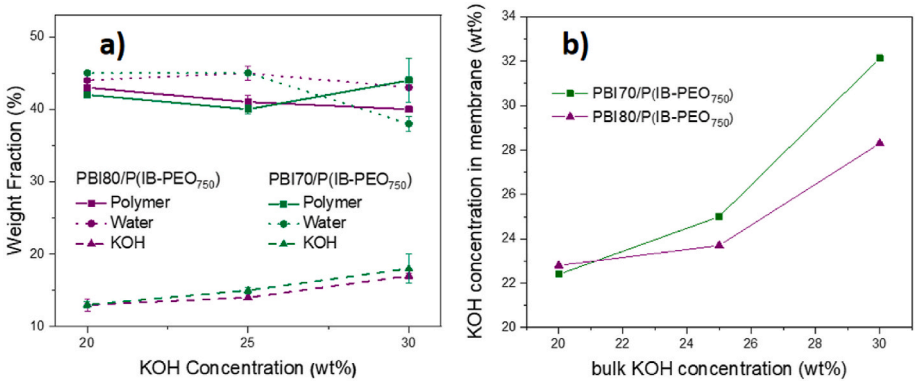

Fig. 6. a) Composition of PBI80/P(IB-PEO$_{750}$) and PBI70/P(IB-PEO$_{750}$) in 20–30 wt% KOH at 80 °C (the markers show the average of three samples, and the error bars represent the standard deviation) and b) concentration of the absorbed solution in the blend membranes.

concentration increase [28] (as discussed later). For comparison, pristine *m*-PBI peaked around 110–120 wt% in 25–30 wt% KOH while pristine P(IB-PEO$_{750}$)-*20* copolymer peaked at 78 wt% in 20 wt% KOH. In addition, the corresponding blend (with *m*-PBI composition 80 wt%) containing copolymer with lower molecular weight PEO (MW 350) peaked at 130 % in 30 wt% KOH under the same experimental conditions (not shown).

The thickness and area swelling behavior of blends was studied as a function of KOH concentration, as shown in Fig. 5b. Area swelling gradually decreased with increasing KOH concentration from 20 to 30 wt%. The area swelling peaked at 12 % and 14 % in 20 wt% KOH for blend PBI80/P(IB-PEO) and PBI70/P(IB-PEO), respectively. The observed low area swelling is essential to prevent build-up of stresses in the membrane during electrolysis testing. In contrast, thickness swelling was continuously increased with increasing KOH concentration and peaked at 90 % and 80 % for PBI80/P(IB-PEO$_{750}$) and PBI70/P(IB-PEO$_{750}$) in 30 wt% KOH, respectively. Consequently, both membranes showed anisotropic swelling behavior which is also typical for KOH doped *m*-PBI. This behavior was attributed to the rapid filling of the space between local lamellar structures with KOH solution because of breaking up the hydrogen bonding [41,42]. In the studied systems, the partial ionization of benzimidazole [43] and the full deprotonation of oxindole groups in 20–30 wt% KOH concentrations, releases the extensive interlayer hydrogen bonding, which in turn allows for extensive swelling of the polymer matrix. The same trend was also observed for membrane systems based on polyoxindole after doping with KOH [27].

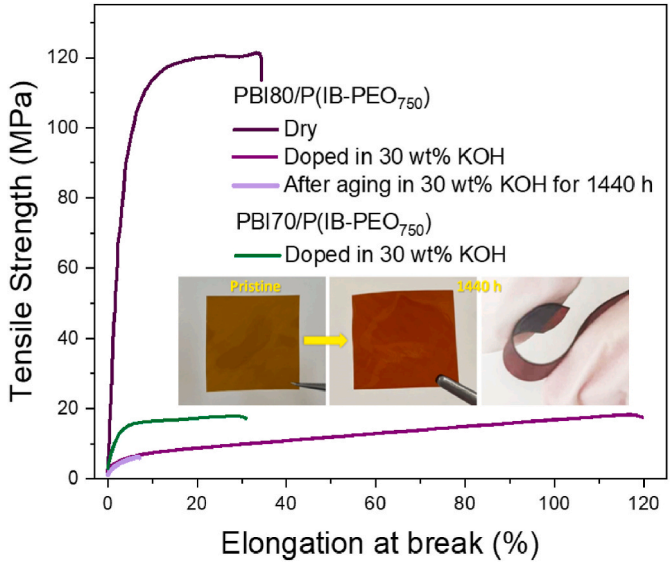

Fig. 7. Stress-strain curves of the blend membranes before and after aging in 30 wt% KOH at 80 °C.

The weight fractions of water, KOH and polymer of the prepared blend membranes after equilibration in 20–30 wt % KOH are depicted in Fig. 6. Generally, a high concentration of KOH electrolyte leads to a high KOH concentration in ISMs. Indeed, the KOH weight fraction was increased from 12 to 17 % for PBI80/P(IB-PEO$_{750}$) and from 10 to 18 % for PBI70/P(IB-PEO$_{750}$), respectively, when KOH surrounding electrolyte concentration increased from 20 wt% to 30 wt% KOH (Fig. 6a). This increase is ascribed to the increased degree of deprotonation of *m*-PBI and to fully ionized oxindole units in this concentration range thus resulting in the formation of negatively charged imidazolide and oxindole ionic moieties enabling the interactions with water and K^+ which in turn allow to absorb freer and bond alkali. This tendency is consistent with that observed for pristine *m*-PBI which displayed the highest KOH content (18 %) at the highest KOH concentration (30 wt%), recorded under the same testing conditions (Fig. S6 of SI).

As for the water weight fraction, both blend membranes followed the same trend, reaching their maximum value of 45 % in 25 wt% KOH solution (Fig. 6a) which is substantially higher than those of pristine *m*-PBI and poly(oxindole biphenylene) polymers (39 % and 23 %, respectively), suggesting that the presence of hydrophilic PEO groups facilitates water absorption. When the KOH electrolyte concentration was further increased to 30 wt%, the water content was slightly decreased for both blends. This is happening because the concentration of water in the surrounding KOH solution decreases with increasing KOH concentration, and the high ionic strength of the surrounding (bulk) KOH solution results in membrane's water uptake decrease due to increased osmotic pressure.

The concentration of the absorbed KOH solution inside the blend membranes can be calculated based on the weight of KOH relative to the combined mass of KOH and water. Interestingly, as shown in Fig. 6b the concentration of KOH solution inside the blend membranes was similar with the KOH concentration of the bulk solution throughout the whole concentration range. For the blend PBI70/P(IB-PEO$_{750}$), the concentration inside the membrane was ≈2.2 wt% higher than that of the bulk solution of 20 and 30 wt% KOH. The same behavior was also observed for *m*-PBI, where for higher than 15 wt% KOH concentration the formal composition inside the membrane was higher than in the external solution [43].

Contact angle data revealed that the wettability was increased with increasing KOH surrounding electrolyte concentration (Fig. S7 of SI), further supporting the above findings. The prepared blends had hydrophilic nature in the dry state as they displayed contact angle values in the range of 66.2°–74.2°, in contrast with pristine *m*-PBI which is more hydrophobic (85°). This stems from the presence of hydrophilic PEO facilitating interactions with water. The maximum wettability of the

Table 2
Summary of mechanical properties of pristine and alkali doped blend membranes.

Membrane	state	Tensile strength (MPa)	Elongation at break (%)	Young's Modulus (MPa)
m-PBI[a]	dry	160 ± 40	4 ± 1	4870 ± 785
P(IB-PEO_{750})-*20*	dry	29 ± 10	2 ± 1	1633 ± 325
PBI80/P(IB-PEO_{350})[a]	dry	159 ± 25	4 ± 1	5212 ± 881
PBI80/P(IB-PEO_{750})	dry	117 ± 3	35 ± 14	2982 ± 620
m-PBI	doped in 30 wt% KOH	11 ± 3	255 ± 13	316 ± 23
PBI80/P(IB-PEO_{750})	doped in 30 wt% KOH	18 ± 1	121 ± 20	186 ± 36
PBI70/P(IB-PEO_{750})	doped in 30 wt% KOH	18 ± 1	32 ± 10	554 ± 68
PBI80/P(IB-PEO_{750})	Aged in 30 wt% KOH for 1440 h	6 ± 0	7 ± 1	197 ± 31

[a] The data are taken from previous work [17].

prepared blends corresponding to the lowest values of 19.1° and 14.9° for PBI80/P(IB-PEO_{750}) and PBI70/P(IB-PEO_{750}), respectively was observed after equilibration in 30 wt% KOH (Fig. S7).

XRD results unveiled that while pristine *m*-PBI showed an amorphous peak at around $2\theta = 25°$ (not shown) with d-spacing = 3.54 Å, this peak became broader and shifted at around $2\theta = 22°$ for blends with a corresponding *d*-spacing of 4.04 Å, as calculated using Bragg's law (Fig. S8 of SI). This suggests that the inter-segmental distance between polymer chains in the case of blends is larger than the corresponding of pristine *m*-PBI which has a tight, close chain packing [43]. The presence of long side PEO groups introduces bulkiness, which can increase *d* spacing. After equilibration of the blend membranes in 20–30 wt% KOH, the peak disappeared, as electrolyte filled the volume between polymer chains thus resulting in polymer chain expansion (loose polymer chain packing). These data further support the anisotropic swelling behavior observed (Fig. 5b).

3.2.2. Mechanical properties

Fig. 7 presents the stress-strain curves of the blend membranes before and after equilibration in 30 % KOH, respectively. The corresponding tensile strength, elongation at break and elastic modulus are given in Table 2. Before equilibration in aqueous KOH, the tensile strength of *m*-PBI reached at 160 MPa and the elongation at break at 4 %, stemming from the strong intermolecular hydrogen bonding between –N = and –NH– segments. The tensile strength of neat P(IB-PEO_{750})-*20* copolymer was much lower (29 MPa, Table 2) than that of neat *m*-PBI due to its weak intermolecular interactions associated with its loose chain packing. Upon blending, the tensile strength was reduced to 117 MPa for PBI80/P(IB-PEO_{750}) but still indicating its high strength while the elongation at break significantly increased (35 %). The inferior tensile strength of the blend compared to that of neat *m*-PBI originates from the disruption of the tight packing of *m*-PBI chains induced by the presence of the flexible PEO side chains which resulted in increased chain spacing via weakening of the strong intermolecular hydrogen bonding of *m*-PBI chains. At the same time, the elastic modulus was decreased due to the plasticization effect induced by the presence of long hydrophilic PEO side chains (MW 750).

It is worth mentioning that the same blend but with shorter PEO groups (MW 350) showed almost the same tensile strength, elongation at break and even higher elastic modulus values compared with pristine *m*-PBI (Table 2), associated with enhanced interchain interactions like hydrogen bonding between the two polymers [17].

After equilibration in 30 wt% KOH, the tensile strength of PBI80/P(IB-PEO_{750}) dropped from 117 MPa to 18 MPa which is higher than that of *m*-PBI (11 MPa), highlighting its improved mechanical strength. From a practical perspective, this decrease is partially compensated by an increased elongation at break from 35 % to 121 %, i.e. already small stresses result in deformation, but only a large strain leads to membrane failure. This is a consequence of the significant absorption of KOH solution enabling the high degree of plastic deformation. This finding agrees well with other PBI-based ISMs [28,41,44]. The strong plasticization of the blend was also evident from the dramatic decrease in elastic modulus from 2982 to 186 MPa. The doped PBI70/P(IB-PEO_{750}) showed the same tensile strength but significantly higher Young' modulus than doped PBI80/P(IB-PEO_{750}). For comparison, the tensile strength values reported in this work are higher or comparable with other reported ISM systems [28,45,46]. For example, blends of *m*-PBI with poly (isatin biphenyl) containing 95-75 wt% *m*-PBI displayed tensile strength in the range of 5–15 MPa after equilibration in 30 wt% KOH [28]. In summary, it can be stated that blending of P(IB-PEO_{750})-*20* copolymer with *m*-PBI increases the mechanical properties of the KOH doped membranes which are high enough for use in AWE despite their high KOH and water fractions.

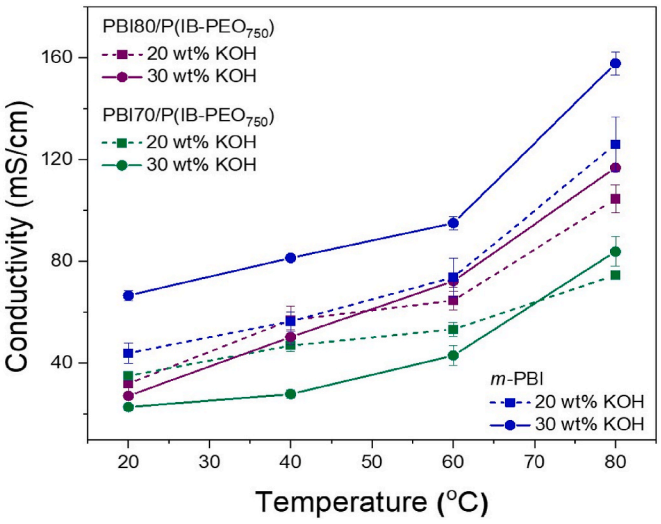

Fig. 8. Ionic conductivity of the blend membranes in two different concentrations of aqueous KOH solution at different temperatures. The markers show the average of two samples, and the error bars represent the standard deviation.

3.2.3. Ionic conductivity

The conductivity of the ion-solvating membranes mainly depends on the absorbed KOH solution and thus is based on both potassium and hydroxide conductivity. So, it is influenced by the concentration of the absorbed KOH solution (the maximum conductivity of KOH solution at room temperature is around 25–30 wt% and is shifted to higher concentrations with increasing temperature [47]), the morphology of the membrane and the weight ratio of absorbed KOH solution to polymer. The through-plane ionic conductivity of blend membranes was measured as a function of temperature at two different KOH concentrations of 20 wt% and 30 wt%, respectively (Fig. 8). The conductivity increases with increasing temperature for both blends. At all temperatures (except 20 °C), PBI80/P(IB-PEO_{750}) membrane displayed higher conductivity than PBI70/P(IB-PEO_{750}) membrane in both KOH concentrations. At 80 °C, the former peaked around 117 mS cm^{-1} while the latter around 84 mS cm^{-1} in 30 wt% KOH solution stemming from its higher electrolyte absorption and increased ion mobility at elevated temperatures. *m*-PBI showed higher conductivity in 30 wt% KOH across the entire temperature range with a maximum value of 158 mS cm^{-1} at 80 °C. The conductivity of PBI80/P(IB-PEO_{750}) was slightly lower compared to that of *m*-PBI despite its higher electrolyte uptake. This can

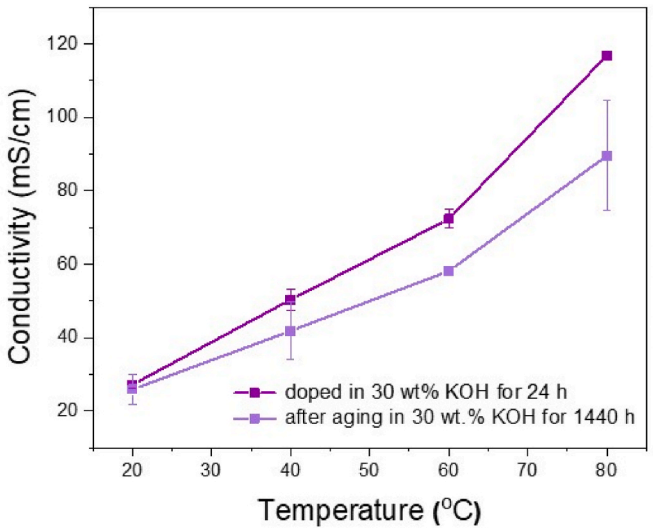

Fig. 9. Ionic conductivity of the PBI80/P(IB-PEO_{750}) membrane during aging for 24 h and for 1440 h in 30 wt % KOH solution at 80 °C. The markers show the average of two samples, and the error bars represent the standard deviation.

be attributed to strong attractive intermolecular interactions between blend components that could negatively affect the ion mobility.

Interestingly, the higher KOH concentration (30 wt%) resulted in higher ionic conductivities for PBI80/P(IB-PEO_{750}) and PBI70/P(IB-PEO_{750}) membranes only at temperatures higher than ~50 °C and ~70 °C, respectively. This behavior is probably associated with increased plasticization (due to the increased electrolyte uptake with increasing temperature) and morphological changes that occur at elevated temperatures enabling the rearrangement of polymer chains and the formation of more open, continuous ionic pathways for ion transport. For comparison, the PBI80/P(IB-PEO_{350}) blend membrane which contains shorter PEO side groups with a molecular weight of 350, exhibited a lower conductivity value (95 mS cm^{-1}) compared to the corresponding PBI80/P(IB-PEO_{750}) blend with longer PEO groups (MW 750) in 30 wt% KOH at 80 °C owing to its lower electrolyte uptake (130 wt% in 30 wt% KOH).

3.2.4. *Alkaline stability*

As PBI80/P(IB-PEO_{750}) showed a suitable balance between high ionic conductivity and mechanical robustness, it was chosen for alkaline stability and electrolysis testing. Hence, the prepared blend membrane was immersed in 30 wt% aqueous KOH at 80 °C for 1440 h to investigate its ex-situ alkaline stability by recording the variations in properties such as ionic conductivity, mechanical properties, thermal stability and chemical structure. Aged PBI80/P(IB-PEO_{750}) membrane remained visually intact, maintaining its mechanical robustness and flexibility (inset, Fig. 7). In addition, no discoloration of the KOH solution was observed, suggesting that no blend material was dissolved to the solution.

The mechanical properties of the aged KOH doped sample were studied. The tensile strength was significantly reduced by 67 % (6 MPa) while Young's modulus slightly increased (197 MPa) after aging (Table 2, Fig. 7). For comparison, both tensile strength and Young's modulus of pristine *m*-PBI was reported to decrease from 94 MPa to 7.6 MPa and from 2554 MPa to 404 MPa after 74 days of testing in 6 M (ca. 27 wt%) KOH at 85 °C [48]. Similar values were also reported for *m*-PBI/FAA3 blend after aging for 4 weeks at 85 °C in 25 wt% KOH solution [45].

The ionic conductivity of the aged sample was recorded in 30 wt% KOH at different temperatures, as illustrated in Fig. 9. The ionic conductivity remained unchanged at 20 °C while a small decline was observed as a function of temperature peaking at 89.6 mS cm^{-1} at 80 °C.

The aged sample (after washing with water and drying) was insoluble in DMSO-d_6, suggesting that cross-links possibly or stronger association of the polymer chains were formed during the stress test in KOH. Thus, ^{1}HNMR study of the aged sample was not possible. A comparison of the ATR-IR spectra before and after aging (Fig. 10a) did not indicate degradation, as no new signals which would suggest hydrolysis of the imidazole rings or hydroxide attack to C2 carbonyl group of isatin were observed. The alkaline stability is further supported by the participation of *m*-PBI's imidazolide and isatin groups with K^+ in attractive interactions. In particular, the band at 1610 cm^{-1} corresponding to C═N stretching of *m*-PBI was broadened and split suggesting enhanced interactions, like hydrogen bonding between imidazole units with potassium imidazolide [43] or with isatin (Fig. S9 of SI). Also, the peak at 1702 cm^{-1} corresponding to the carbonyl group of isatin became broader and the shoulder observed at 1689 cm^{-1} shifted to lower wavenumbers (1687 cm^{-1}) indicating hydrogen bond formation or ionic interaction with K^+. Similar findings were also reported in our previous work for PBI80/P(IB-PEO_{350}) blend membrane supporting its excellent stability after exposure in 20 wt% KOH at 80 °C for one month [17].

TGA results (Fig. 10b) further support ATR-IR findings since the aged blend showed significantly improved thermo-oxidative stability, especially at temperature higher than 300 °C. While the weight loss around 300 °C in the pristine copolymer was attributed to the PEO groups decomposition, after aging no weight loss was observed in this temperature, suggesting significant intermolecular forces between the blend components. One possible explanation is that PEO groups ionically interact with K^+ and *m*-PBI's imidazolide groups. To conclude, the excellent alkaline stability of the blend could be attributed to the strong attractive electrostatic interactions, which are also matched with the conductivity test results. Taking this into consideration, the

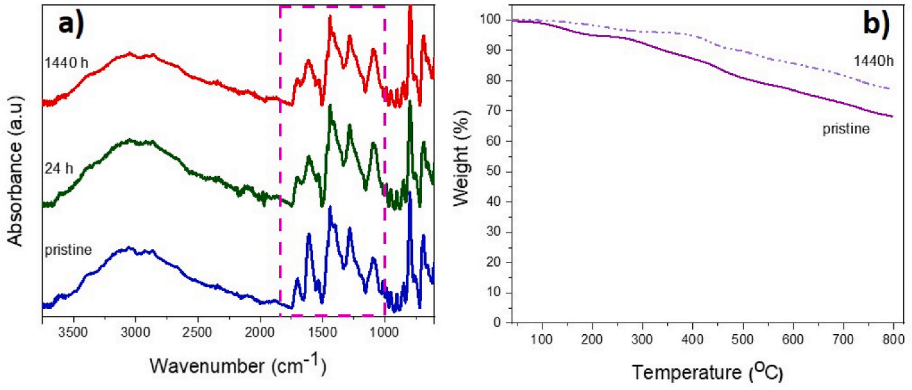

Fig. 10. a) ATR spectra b) TGA curves of the untreated PBI80/P(IB-PEO_{750}) membrane and the corresponding membrane after aging (washed and dried) for 24 h and for 1440 h in 30 wt % KOH solution at 80 °C.

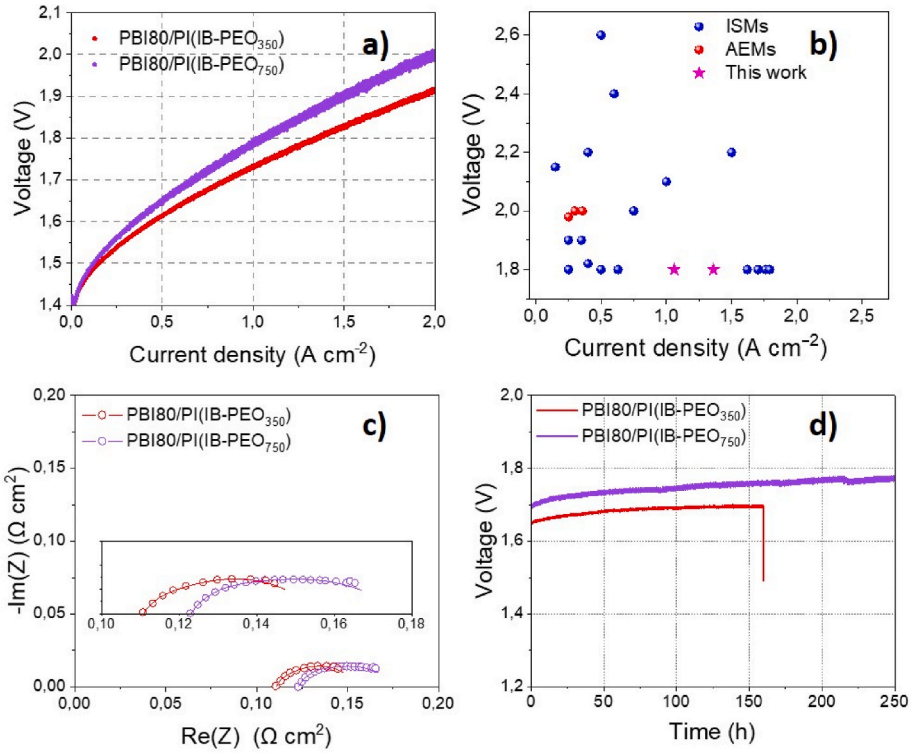

Fig. 11. Electrochemical characterization of the AWE cell with Raney Nickel-based electrodes, with PBI80/P(IB-PEO_{350}) and PBI80/P(IB-PEO_{750}) membranes in 30 wt% KOH at 80 °C: a) cell-voltage curves, b) comparison of the electrochemical performance of the blends prepared in this work with other reported ISMs and AEMs based systems [17,18,20,24,25,27,29,40,43,45,51–53], c) Nyquist plots from the EIS measurements and their fittings for cells with different membranes at 2 A cm^{-2}, the magnified Nyquist plots are shown in the inset and d) Long-term durability test of cells with PBI80/P(IB-PEO_{350}) and PBI80/P(IB-PEO_{750}) membranes in 30 wt% KOH at 80 °C at a constant current density of 0.5 A cm^{-2}.

deterioration of mechanical properties after aging was not caused by chemical degradation but by structural changes in polymer blend morphology, as already reported [45]. In specific, the prolonged KOH treatment at elevated temperatures enables the enhanced release of the strong hydrogen bonding network between the –N = and –NH– segments of *m*-PBI and the formation of much weaker interactions bridging *m*-PBI's imidazolide groups and PEO/isatin with doped alkali which in turn result in mechanical strength deterioration [44].

3.2.5. *Electrolysis testing*

Fig. 11a shows the polarization curves of the AWE cells with the PBI80/P(IB-PEO_{750}) and PBI80/P(IB-PEO_{350}) membranes for comparison. Both cells used the same electrodes (Raney Nickel-based electrodes) and operated in atmospheric pressure in 30 wt% KOH at 80 °C. The cell with the PBI80/P(IB-PEO_{350}) membrane displayed the higher current density of approximately 1.36 A cm^{-2} at 1.8 V while the cell with the PBI80/P(IB-PEO_{750}) membrane showed a lower current density of 1.06 A cm^{-2} at 1.8 V. Therefore, a lower cell voltage over the entire current densities range was observed for the AWE with PBI80/P(IB-PEO_{350}) membrane. The performance of cells with both membranes is comparable or even outperforms most of the membranes and Zirfon previously reported in the literatures [18,20,24,25,27–29,40,45,51–53]. A comparison of the performances of different representative ISM- and AEM-based alkaline electrolysis systems using non-noble metal catalysts is given in Fig. 11b. For example, the performance of both cells with PBI80/P(IB-PEO_{750}) and PBI80/P(IB-PEO_{350}) membranes exceeds that of commercial separator Zirfon using Raney Nickel based electrodes in 24 wt% KOH at 80 °C (0.63 A cm^{-2} at 1.8 V) and for blend PBI80/P (IB-PEO_{350}) is comparable with that of *m*-PBI (1.7 A cm^{-2} at 1.8 V) [20]. In addition, *m*-PBI/FAA3 blends showed a current density of 1 A cm^{-2} at 2.55 V in 20 wt% at 60 °C [45] while blends of *m*-PBI with poly (isatin biphenyl) displayed a current density of 0.4 A cm^{-2} at 2.2 V in 6 M KOH at 80 °C [28] (both using Nickel foam electrodes), highlighting the excellent performance of the prepared blend membranes. To further understand the effect of using different membranes on the overall cell performance, EIS was collected at 2 A cm^{-2}, where the cell performance is directly governed mainly by the membrane properties. Fig. 11c shows the impedance analysis together with their model fits (Fig. S10 of SI) as a Nyquist plot for cells with different membranes at high current densities of 2 A cm^{-2}. The impedance data collected at 2 A cm^{-2} (Fig. 11c) shows that the R_{ohm} or high frequency resistance appearing as the intercept of the Nyquist plots with the x-axis at high frequency (left side of Nyquist plot), which arises mainly from solution and membrane resistance is affected by changing the membranes in the cell. Quantification of the resistance associated to the high frequency region indicates a decreased R_{ohm} value, when PBI80/P(IB-PEO_{750}) is replaced by PBI80/P (IB-PEO_{350}) membrane. Fig. 11c shows that cell with PBI80/P (IB-PEO_{350}) membrane showed lower ohmic resistance compared to the cell with PBI80/P(IB-PEO_{750}), which is in line with the polarization curves. In detail, the ohmic resistances, which are mainly governed by membrane properties were fitted as ≈ 0.107 Ω cm^2 for PBI80/P (IB-PEO_{350}) and ≈0.117 Ω cm^2 for PBI80/P(IB-PEO_{750}). The higher ohmic resistance of the latter one probably originates from its softer nature (due to its higher electrolyte uptake) that is more compressed into the electrode pores than PBI80/P(IB-PEO_{350}) thus on one hand, making bubble removal less efficient and on the other hand could also result in reduced number of catalytic sites, ultimately leading to decreased overall performance. This is also in agreement with high frequency resistance obtained from the Bode plots at 2 A cm^{-2}, Fig. S11a and S11b of SI. The resistance associated with the medium and low frequency arc related to the electrode kinetics was relatively small and in the range of 0.009–0.014 Ω cm^2 for R_c and 0.038–0.044 Ω cm^2 for R_a for both cells with different membranes. The high frequency resistance is estimated from the Bode plots (corresponding to a phase angle close to

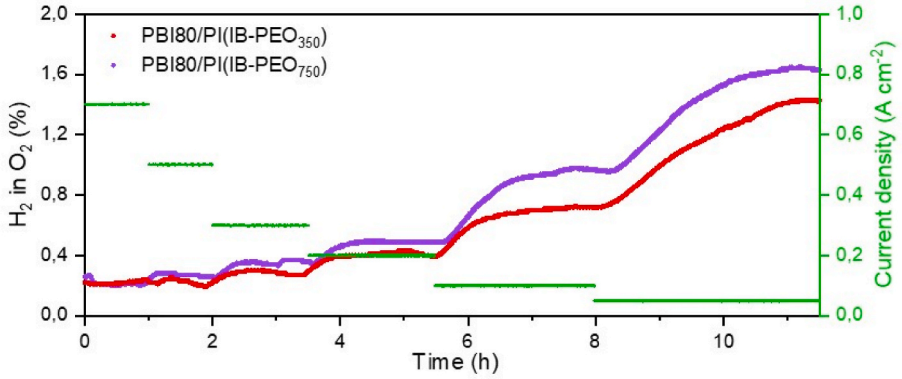

Fig. 12. Gas purity: hydrogen in oxygen levels over wide range of current densities for cells with both PBI80/P(IB-PEO_{350}) and PBI80/P(IB-PEO_{750}) membranes in 30 wt% KOH at 80 °C.

zero) [49]. Bode plots consist of plots of the magnitude of the impedance and phase as a function of frequency [49]. Proven by Bode plot, R_{ohm}, in Fig. S11a and S11b of SI reduced when PBI80/P(IB-PEO_{750}) is replaced by PBI80/P(IB-PEO_{350}) membrane. Long-term durability tests for both membranes, PBI80/P(IB-PEO_{350}) and PBI80/P(IB-PEO_{750}) were conducted in 30 wt% KOH at 80 °C beginning with a 24h AST test, followed by a durability test at a constant current density of 0.5 A cm^{-2}. AST tests, in which the cells were cycling in a very harsh condition between low and high current densities (see experimental section) show negligible voltage increment for both cells with different membranes, Fig. S12a and S12b of SI. Afterwards the cells were kept at a constant current density of 0.5 A cm^{-2} for long-term durability test. The cell-voltage changes as a function of time are shown in Fig. 11d. Both the cells showed initial slight increment in voltage, which is reported to be due to the bubble formation and partially electrode surface coverage at the beginning of the test [50]. However, the voltage becomes more stable after few hours and later slight increment in voltage was observed in both cells. In contrast to the cell with PBI80/P(IB-PEO_{350}), which failed after 160 h, the cell with PBI80/P(IB-PEO_{750}) membrane successfully run for 250 h, showing its applicability for harsh alkaline conditions of AWE. More efforts are needed to further improve the durability of PBI80/P(IB-PEO_{350}) membrane in the future work.

The gas purity was measured for the cells with two different membranes in 30 wt% KOH at 80 °C (Fig. 12). It is reported that the amount of hydrogen transferred to oxygen is much larger than the amount of oxygen transferred to hydrogen side [54]. Hydrogen permeation is an important phenomenon for AWE, due to several reasons related to safety issues and efficiency loss. Fig. 12 shows the H_2 in O_2 content in a wide current density range up to 0.7 A cm^{-2} for the cells with two different membranes. For both cells with two different synthesized membranes in this work, the H_2 in O_2 contents at low current densities displayed 1.4–1.65 vol%, which satisfies a chosen safety limit of 2 vol% H_2 in O_2, which is about half of the previously mentioned lower explosion limit (LEL) of ≈4 vol% H_2 in O_2 [55]. The above results showed promising cell performance for both membranes with high gas purity. To conclude, further work in the future will be conducted on the optimization of the performance of the prepared ion-solvating membranes while maintaining their high chemical stability and high H_2 barrier property.

4. Conclusions

This study presents a promising approach toward high performance ISMs using a polymer blend strategy. Novel PEO functionalized polyoxindole copolymers bearing the ion solvating, long PEO sequences (MW750) as side chains were synthesized using a functionalized monomer strategy followed by super-acid polyhydroxyalkylation. The prepared copolymers due to their increased plasticization caused by their high electrolyte uptakes were blended with *m*-PBI to afford mechanically stable membranes. By adjusting the ratio of P(IB-PEO_{750})-*20* to *m*-PBI, highly conductive membranes with excellent mechanical properties were obtained. Blend membrane PBI80/P(IB-PEO_{750}) was still flexible and retained its initial conductivity after KOH exposure for 2 months in 30 wt% KOH at 80 °C, indicating its excellent alkaline stability. This was attributed to the blend stabilization by the formation of strong attractive interactions and ionic cross-links between blend components as revealed by ATR-IR analysis. This result was on par with the TGA analysis which showed improved thermo-oxidative stability of the aged sample. Finally, the blend membrane PBI80/P(IB-PEO_{750}) was successfully tested in an alkaline water electrolyzer, exhibiting a promising performance of 1.06 A cm^{-2} at 1.8 V in 30 wt% KOH at 80 °C outperforming commercial separator Zirfon. To study the effect of membrane on the performance, the PBI80/P(IB-PEO_{350}) membrane with shorter PEO chains was also tested showing a higher performance of 1.36 A cm^{-2} at 1.8 V under the same conditions. The latter compares well with that of *m*-PBI and also exceeds that of commercial separator Zirfon. In addition, both blend membranes displayed H_2 in O_2 contents of 1.4–1.65 vol% at low current densities, which are low enough to satisfy safety limits while the cell with PBI80/P(IB-PEO_{750}) membrane showed stable performance for 250 h. Consequently, this study demonstrated the potential of the prepared ISM membranes by a simple blending method in AWE application.

CRediT authorship contribution statement

Sara Gjoshi: Writing – original draft, Visualization, Methodology, Investigation, Data curation. **Charalampos Anastasopoulos:** Methodology, Investigation. **Kamal Ghotia:** Methodology, Investigation, Data curation. **Davide Grilli:** Methodology, Investigation, Data curation. **Franz Egert:** Visualization, Methodology, Investigation. **Syed Asif Ansar:** Supervision, Resources, Funding acquisition. **Fatemeh Razmjooei:** Writing – review & editing, Writing – original draft, Validation, Supervision, Resources, Methodology, Data curation. **Valadoula Deimede:** Writing – review & editing, Writing – original draft, Visualization, Validation, Supervision, Resources, Methodology, Conceptualization.

Declaration of competing interest

The authors declare that they have no known competing financial interests or personal relationships that could have appeared to influence the work reported in this paper.

Acknowledgments

This work was financially supported by the European Union's Horizon 2020 Research and Innovation Action program "Materials for next

generation of alkaline electrolyzer" (NEXTAEC), grant agreement 862509 and this work was also supported by the project 'Pressurized Efficient Alkaline Electrolyser (PEACE)', funded under the Horizon Europe programme (Grant Agreement No. 101101343) by the Clean Hydrogen Partnership and its members. The authors are grateful to Assoc. Prof. A. Kalarakis (Department of Mechanical Engineering, University of the Peloponnese) for SEM measurements.

Appendix A. Supplementary data

Supplementary data to this article can be found online at https://doi.org/10.1016/j.memsci.2025.124368.

Data availability

Data will be made available on request.

References

[1] H.A. Miller, K. Bouzek, J. Hnat, S. Loos, C.I. Bernäcker, T. Weißgärber, L. Röntzsch, J. Meier-Haack, Green hydrogen from anion exchange membrane water electrolysis: a review of recent developments in critical materials and operating conditions, Sustain. Energy Fuels 4 (5) (2020) 2114–2133.
[2] J. Brauns, T. Turek, Alkaline water electrolysis powered by renewable energy: a review, Processes 8 (2020) 248.
[3] G.A. Lindquist, Q. Xu, S.Z. Oener, S.W. Boettcher, Membrane electrolyzers for impure-water splitting, Joule 4 (12) (2020) 2549–2561.
[4] F. Rocha, C. Georgiadis, K. Van Droogenbroek, R. Delmelle, X. Pinon, G. Pyka, G. Kerckhofs, F. Egert, F. Razmjooei, S.-A. Ansar, S. Mitsushima, J. Proost, Proton exchange membrane-like alkaline water electrolysis using flow-engineered three-dimensional electrodes, Nat. Commun. 15 (2024) 7444.
[5] T. Jiang, X. Jiang, J. Hnat, A. Michalkova, I. Biswas, R. Reissner, V. Kyriakou, F. Razmjooei, H. Liao, K. Bouzek, S.-A. Ansar, One step electrochemical fabrication of high performance Ni@Fe-doped Ni(oxy)hydroxide anode for practical alkaline water electrolysis, J. Mater. Chem. A 10 (2022) 23863–23873.
[6] L.P. Campo Schneider, M. Dhrioua, D. Ullmer, F. Egert, H.J. Wiggenhauser, K. Ghotia, N. Kawerau, D. Grilli, F. Razmjooei, S.-A. Ansar, Advancements in hydrogen production using alkaline electrolysis systems: a short review on experimental and simulation studies, Curr. Opin. Electrochem. 47 (2024) 101552.
[7] V. Deimede, D. Labou, S.G. Neophytides, Polymer electrolyte membranes based on blends of sulfonated polysulfone and PEO-grafted polyethersulfone for low temperature water electrolysis, J. Appl. Polym. Sci. 131 (2014) 39922.
[8] M. Carmo, D.L. Fritz, J. Mergel, D. Stolten, A comprehensive review on PEM water electrolysis, Int. J. Hydrogen Energy 38 (12) (2013) 4901–4934.
[9] D. Aili, M.R. Kraglund, S.C. Rajappan, D. Serhiichuk, Y. Xia, V. Deimede, J. Kallitsis, C. Bae, P. Jannasch, D. Henkensmeier, J.O. Jensen, Electrode separators for the next-generation alkaline water electrolyzers, ACS Energy Lett. 8 (4) (2023) 1900–1910.
[10] F. Egert, D. Ullmer, S. Marx, E. Taghizadeh, T. Morawietz, M. Gerle, T. Anh Le, L. P. Campo Schneider, I. Shubir Biswas, R.E. Wirz, P. Spieth, T. Marquard-Möllenstedt, A. Brinner, R. Faccio, L. Fernández-Werner, M. Esteves, F. Razmjooei, S.A. Ansar, Intensification of alkaline electrolyzer with improved two-phase flow, Adv. Energy Mater. (2025) 2405285.
[11] D. Li, A.R. Motz, C. Bae, C. Fujimoto, G. Yang, F.-Y. Zhang, K.E. Ayers, Y.S. Kim, Durability of anion exchange membrane water electrolyzers, Energy Environ. Sci. 14 (6) (2021) 3393–3419.
[12] E.J. Park, P. Jannasch, K. Miyatake, C. Bae, K. Noonan, C. Fujimoto, S. Holdcroft, J. R. Varcoe, D. Henkensmeier, M.D. Guiver, Y.S. Kim, Aryl ether-free polymer electrolytes for electrochemical and energy devices, Chem. Soc. Rev. 53 (11) (2024) 5704–5780.
[13] D. Henkensmeier, W.-C. Cho, P. Jannasch, J. Stojadinovic, Q. Li, D. Aili, J. O. Jensen, Separators and membranes for advanced alkaline water electrolysis, Chem. Rev. 124 (10) (2024) 6393–6443.
[14] J. Choi, H. Kim, S. Jeon, M.G. Shin, J.Y. Seo, Y.I. Park, A.S. Lee, C. Lee, M. Kim, H. S. Cho, J.H. Lee, Thin film composite membranes as a new category of alkaline water electrolysis membranes, Small 19 (37) (2023) 2300825.
[15] W. Song, K. Peng, W. Xu, X. Liu, H. Zhang, X. Liang, T. Xu, Upscaled production of an ultramicroporous anion-exchange membrane enables long-term operation in electrochemical energy devices, Nat. Commun. 14 (2023) 2732.
[16] J. Jung, Y.S. Park, D.J. Hwang, G.H. Choi, D.H. Choi, H.J. Park, C.-H. Ahn, S. S. Hwang, A.S. Lee, Polydiallylammonium interpenetrating cationic network ion-solvating membranes for anion exchange membrane water electrolyzers, J. Mater. Chem. A 11 (2023) 10891–10900.
[17] M. Makrygianni, S. Aivali, Y. Xia, M.R. Kraglund, D. Aili, V. Deimede, Polyisatin derived ion-solvating blend membranes for alkaline water electrolysis, J. Membr. Sci. 669 (2023) 121331.
[18] Q. Chen, Y. Huang, X. Hu, B. Hu, M. Liu, J. Bi, L. Liu, N. Li, A novel ion-solvating polymer electrolyte based on imidazole-containing polymers for alkaline water electrolysis, J. Membr. Sci. 668 (2023) 121186.
[19] M.R. Kraglund, D. Aili, K. Jankova, E. Christensen, Q. Li, J.O. Jensen, Zero-gap alkaline water electrolysis using ion-solvating polymer electrolyte membranes at reduced KOH concentrations, J. Electrochem. Soc. 163 (11) (2016) F3125.
[20] M.R. Kraglund, M. Carmo, G. Schiller, S.A. Ansar, D. Aili, E. Christensen, J. O. Jensen, Ion-solvating membranes as a new approach towards high rate alkaline electrolyzers, Energy Environ. Sci. 12 (11) (2019) 3313–3318.
[21] D. Aili, K. Jankova, Q. Li, N.J. Bjerrum, J.O. Jensen, The stability of poly(2,2′-(m-phenylene)-5,5′-bibenzimidazole) membranes in aqueous potassium hydroxide, J. Membr. Sci. 492 (2015) 422–429.
[22] D. Serhiichuk, T. Patniboon, Y. Xia, M.R. Kraglund, J.O. Jensen, H.A. Hansen, D. Aili, Insight into the alkaline stability of arylene-linked bis-benzimidazoles and polybenzimidazoles, ACS Appl. Polym. Mater. 5 (1) (2023) 803–814.
[23] B. Hu, Y. Huang, L. Liu, X. Hu, K. Geng, Q. Ju, M. Liu, J. Bi, S. Luo, N. Li, A stable ion-solvating PBI electrolyte enabled by sterically bulky naphthalene for alkaline water electrolysis, J. Membr. Sci. 643 (2022) 120042.
[24] R. Gao, Y. Wang, M. Liu, B. Hu, M. Liu, E. Yang, X. Zhou, L. Chen, Y. Huang, J. Yao, Q. Zhang, N. Li, Optimization of alkaline water electrolysis performance with binaphthyl-derived polybenzimidazole ion-solvating gel membrane, J. Membr. Sci. 663 (2025) 121005.
[25] D. Serhiichuk, D. Tian, M.R. Almind, Z. Ma, Y. Xia, M.R. Kraglund, C. Bae, J. O. Jensen, D. Aili, Carboxylated Polystyrene-b-poly(ethylene-ran-butylene)-b-polystyrene membranes for alkaline water electrolysis, ACS Appl. Energy Mater. 7 (3) (2024) 1080–1091.
[26] E.J. Park, S. Maurya, M.R. Hibbs, C.H. Fujimoto, K.-D. Kreuer, Y.S. Kim, Alkaline stability of quaternized diels-alder polyphenylenes, Macromolecules 52 (14) (2019) 5419–5428.
[27] X. Hu, B. Hu, C. Niu, J. Yao, M. Liu, H. Tao, Y. Huang, S. Kang, K. Geng, N. Li, An operationally broadened alkaline water electrolyser enabled by highly stable poly (oxindole biphenylene) ion-solvating membranes, Nat. Energy 9 (4) (2024) 401–410.
[28] Y. Xia, B. Abu Sara, S.C. Rajappan, D. Serhiichuk, M.R. Kraglund, J.O. Jensen, V. Deimede, D. Aili, Macromolecular reinforcement of alkaline ion-solvating polymer electrolytes, Polymer 302 (2024) 127068.
[29] S. Gjoshi, P. Loukopoulou, M. Plevova, J. Hnat, K. Bouzek, V. Deimede, Cycloaliphatic Quaternary ammonium functionalized poly(oxindole biphenyl) based anion-exchange membranes for water electrolysis: stability and performance, Polymers 16 (1) (2024) 99.
[30] A. Ioannidi, D. Vroulias, J. Kallitsis, T. Ioannides, V. Deimede, Synthesis and characterization of poly(ethylene oxide) based copolymer membranes for efficient gas/vapor separation: effect of PEO content and chain length, J. Membr. Sci. 632 (2021) 119353.
[31] A. Vöge, V. Deimede, F. Paloukis, S.G. Neophytides, J.K. Kallitsis, Synthesis and properties of aromatic polyethers containing poly(ethylene oxide) side chains as polymer electrolytes for lithium ion batteries, Mater. Chem. Phys. 148 (1) (2014) 57–66.
[32] D. Aili, A.G. Wright, M.R. Kraglund, K. Jankova, S. Holdcroft, J.O. Jensen, Towards a stable ion-solvating polymer electrolyte for advanced alkaline water electrolysis, J. Mater. Chem. A 5 (10) (2017) 5055–5066.
[33] X. Li, F.C. Walsh, D. Pletcher, Nickel based electrocatalysts for oxygen evolution in high current density, alkaline water electrolysers, Phys. Chem. Chem. Phys. 13 (3) (2011) 1162–1167.
[34] M. Schalenbach, W. Lueke, D. Stolten, Hydrogen diffusivity and electrolyte permeability of the Zirfon PERL separator for alkaline water electrolysis, J. Electrochem. Soc. 163 (14) (2016) F1480.
[35] A. Ioannidi, C. Anastasopoulos, D. Vroulias, J. Kallitsis, T. Ioannides, V. Deimede, Synthesis and properties of polymeric ionic liquids (PILs) bearing hydrophilic PEO groups, Sep. Purif. Technol. 280 (2022) 119790.
[36] M.C.G. Hernandez, M.G. Zolotukhin, S. Fomine, G. Cedillo, S.L. Morales, N. Fröhlich, E. Preis, U. Scherf, M. Salmón, M.I. Chávez, J. Cárdenas, A. Ruiz-Trevino, Novel, Metal-free, superacid-catalyzed "click" reactions of isatins with linear, nonactivated, multiring aromatic hydrocarbons, Macromolecules 43 (17) (2010) 6968–6979.
[37] M.T. Guzmán-Gutiérrez, D.R. Nieto, S. Fomine, S.L. Morales, M.G. Zolotukhin, M.C. G. Hernandez, H. Kricheldorf, E.S. Wilks, Dramatic enhancement of superacid-catalyzed polyhydroxyalkylation reactions, Macromolecules 44 (2) (2011) 194–202.
[38] S. Zhang, X. Zhu, C. Jin, Development of a high-performance anion exchange membrane using poly(isatin biphenylene) with flexible heterocyclic Quaternary ammonium cations for alkaline fuel cells, J. Mater. Chem. A 7 (12) (2019) 6883–6893.
[39] C. Long, T. Zhao, L. Tian, Q. Liu, F. Wang, Z. Wang, H. Zhu, Highly stable and conductive multicationic Poly(biphenyl indole) with extender side chains for anion exchange membrane fuel cells, ACS Appl. Energy Mater. 4 (6) (2021) 6154–6165.
[40] O. Bostrom, S.-Y. Choi, L. Xia, S. Meital, F. Lohmann-Richters, P. Jannasch, Alkali-stable polybenzimidazole anion exchange membranes tethered with *N, N*-dimethylpiperidinium cations for dilute aqueous KOH fed water electrolyzers, J. Mater. Chem. A 11 (2023) 21170.
[41] D. Aili, K. Jankova, J. Han, N.J. Bjerrum, J.O. Jensen, Q. Li, Understanding ternary poly(potassium benzimidazolide)-based polymer electrolytes, Polymer 84 (2016) 304–310.
[42] E. Babcock, N. Szekely, A. Konovalova, Y. Lin, M.S. Appavou, G. Mangiapia, Z. Revay, C. Stieghorst, O. Holderer, D. Henkensmeier, W. Lehnert, M. Carmo, Using neutron methods SANS and PGAA to study evolution of structure and composition of alkali-doped polybenzimidazole membranes, J. Membr. Sci. 577 (2019) 12–19.

[43] M.L.A. Trisno, A. Dayan, S.J. Lee, F. Egert, M. Gerle, M.R. Kraglund, J.O. Jensen, D. Aili, A. Roznowska, A. Michalak Michalak, H.S. Park, F. Razmjooei, S.A. Ansar, D. Henkensmeier, Reinforced gel-state polybenzimidazole hydrogen separators for alkaline water electrolysis, Energy Environ. Sci. 15 (2022) 4362–4375.
[44] L. Zeng, T.S. Zhao, L. An, G. Zhao, X.H. Yan, Physicochemical properties of alkaline doped polybenzimidazole membranes for anion exchange membrane fuel cells, J. Membr. Sci. 493 (2015) 340–348.
[45] A. Konovalova, H.J. Kim, S. Kim, A. Lim, H.S. Park, M.R. Kraglund, D. Aili, J. H. Jang, H.J. Kim, D. Henkensmeier, Blend membranes of polybenzimidazole and an anion exchange ionomer (FAA3) for alkaline water electrolysis: improved alkaline stability and conductivity, J. Membr. Sci. 564 (2018) 653–662.
[46] B. Hu, Z. Li, L. Liu, M. Liu, Y. Huang, T. Guo, R. Zhang, K. Geng, N. Li, Highly ion conductive ion solvating membranes for durable alkaline water electrolysis at low temperature and voltage, J. Mater. Chem. A 12 (2024) 20449.
[47] R.J. Gilliam, J.W. Graydon, D.W. Kirk, S.J. Thorpe, A review of specific conductivities of potassium hydroxide solutions for various concentrations and temperatures, Int. J. Hydrogen Energy 32 (2007) 359–364.
[48] D. Aili, M.K. Hansen, R.F. Renzaho, Q. Li, E. Christensen, J.O. Jensen, N.J. Bjerrum, Heterogeneous anion conducting membranes based on linear and crosslinked KOH doped polybenzimidazole for alkaline water electrolysis, J. Membr. Sci. 447 (2013) 424–432.
[49] C.G. Arges, V. Ramani, Z. Wang, R.J. Ouimet, Assessing the oxidative stability of anion exchange membranes in oxygen saturated aqueous alkaline solutions, Front. Energy Res. 10 (2022) 871851.
[50] M.I. Zappia, S. Bellani, Y. Zuo, M. Ferri, F. Drago, L. Manna, F. Bonaccorso, High-current density alkaline electrolyzers: the role of Nafion binder content in the catalyst coatings and techno-economic analysis, Front. Chem. 10 (2022) 1045212.
[51] A. Dayan, M.L.A. Trisno, C. Yang, M.R. Kraglund, M.R. Almind, J. Hjelm, J. O. Jensen, D. Aili, H.S. Park, D. Henkensmeier, Quaternary ammonium-free membranes for Water electrolysis with 1 m KOH, Adv. Energy Mater. 13 (46) (2023) 2302966.
[52] X. Hu, M. Liu, Y. Huang, L. Liu, N. Li, Sulfonate-functionalized polybenzimidazole as ion-solvating membrane toward high-performance alkaline water electrolysis, J. Membr. Sci. 663 (2022) 121005.
[53] D. Aili, M.R. Kraglund, J. Tavacoli, C. Chatzichristodoulou, J.O. Jensen, Polysulfone-polyvinylpyrrolidone blend membranes as electrolytes in alkaline water electrolysis, J. Membr. Sci. 598 (2020) 117674.
[54] Impacts of intermittency on low-temperature electrolysis technologies: a comprehensive review, Int. J. Hydrogen Energy 70 (2024) 474–492.
[55] H. Janssen, J.C. Bringmann, B. Emonts, V. Schroeder, Safety-related studies on hydrogen production in high-pressure electrolysers, Int. J. Hydrogen Energy 29 (2004) 759–770.